Oxidation of Low-Density Lipoproteins Induces Amyloid-like Structures That Are Recognized by Macrophages[†]

Cameron R. Stewart,[‡] Anita A. Tseng,[§] Yee-Foong Mok,[‡] Maree K. Staples,[‡] Carl H. Schiesser,[||] Lynne J. Lawrence,[⊥] Jose N. Varghese,[⊥] Kathryn J. Moore,[§] and Geoffrey J. Howlett*[,‡]

Russell Grimwade School of Biochemistry and Molecular Biology, The University of Melbourne, Parkville, Victoria 3010, Australia, Lipid Metabolism Unit, Massachusetts General Hospital, Harvard Medical School, Boston, Massachusetts 02114, School of Chemistry, The University of Melbourne, Parkville, Victoria 3010, Australia, and Commonwealth Scientific and Industrial Research Organization, Parkville, Victoria 3052, Australia

Received March 17, 2005; Revised Manuscript Received April 21, 2005

ABSTRACT: The macrophage scavenger receptor CD36 plays a key role in the initiation of atherosclerosis through its ability to bind to and internalize oxidized low-density lipoproteins (oxLDL). Prompted by recent findings that the CD36 receptor also recognizes amyloid fibrils formed by β-amyloid and apolipoprotein C-II, we investigated whether the oxidation of low-density lipoproteins (LDL) generates characteristic amyloid-like structures and whether these structures serve as CD36 ligands. Our studies demonstrate that LDL oxidized by copper ions, 2,2-azobis(2-amidinopropane) dihydrochloride (AAPH), or ozone react with the diagnostic amyloid dyes thioflavin T and Congo Red and bind to serum amyloid P component (SAP), a universal constituent of physiological amyloid deposits. X-ray powder diffraction patterns for native LDL show a diffuse powder diffraction ring with maximum intensity corresponding to an atomic spacing of ~4.7 Å, consistent with the spacing between β-strands in a β-sheet. Ozone treatment of LDL generates an additional diffuse powder diffraction ring with maximum intensity indicating a spacing of ~9.8 Å. This distance is consistent with the presence of cross-β-structure, a defining characteristic of amyloid. Evidence that these cross-β-amyloid structures in oxLDL are recognized by macrophages is provided by the observation that SAP strongly inhibits the association and internalization of ^{125}I-labeled copper-oxidized LDL by peritoneal macrophages. The ability of SAP to bind to amyloid-like structures in oxLDL and prevent lipid uptake by macrophages highlights the potential importance of these structures and suggests an important preventative role for SAP in foam cell formation and early-stage atherosclerosis.

The uptake of low-density lipoproteins (LDL)[1] by macrophages leads to the arterial deposition of lipid-laden "foam cells" that characterize early-stage atherosclerosis. The observation that patients totally lacking the LDL receptor nevertheless accumulate large amounts of cholesterol in their macrophages (*1*) suggests that circulating LDL must undergo some kind of structural modification before becoming fully proatherogenic. Most attention has focused on oxidative modification and the uptake of oxLDL by the macrophage scavenger receptors, SR-A and CD36 (*2*, *3*). These receptors belong to a family of so-called "pattern recognition" receptors and appear to recognize oxidized phospholipids and protein−lipid adducts generated during oxidation. A monoclonal antibody, EO6, specific for oxidized phosphatidylcholine, binds to intact oxLDL, the isolated apoB from oxLDL, and the isolated lipid moiety from oxLDL and blocks the uptake of oxLDL by CD36 transfected COS-7 cells (*4*). However, despite intensive investigation the oxidized species that mediate the influx of lipids into macrophages remain poorly characterized, and trials of antioxidant therapies fail to show a positive impact on atherosclerosis (*5*). Other types of LDL modification, including mechanically induced LDL aggregation (*6*) and enzyme modification (*7*, *8*), also favor foam cell formation in vitro, suggesting that other types of signal recognition events may be involved. Our recent studies show that CD36 also binds fibrillar β-amyloid, initiating a signaling cascade in macrophages and brain microglia that stimulates the production of inflammatory mediators (*9*, *10*). β-Amyloid fibrils inhibit the binding of oxLDL to macrophages via CD36, but not SRA, receptor-dependent processes (*11*). Apolipoprotein (apo) C-II, a fibrillar amyloid protein present in human atheroma, also initiates macrophage inflammatory responses via the CD36 receptor, including reactive oxygen production and TNF-α expression (*12*). Together, these studies suggested that amyloid species are ligands for the CD36 receptors and that diverse modifications of LDL may generate amyloid-like structures as a common mechanism for receptor-mediated lipid uptake by macrophages.

[†] This work was supported by the Australian Research Council, National Health and Medical Research Council Grant 208913, NIH Grant R01 AG20255, and The Ellison Medical Foundation.

* Correspondence should be addressed to this author. Phone: +61 3 8344 7632. Fax: +61 3 9347 7730. E-mail: ghowlett@unimelb.edu.au.

[‡] Russell Grimwade School of Biochemistry and Molecular Biology, The University of Melbourne.

[§] Massachusetts General Hospital, Harvard Medical School.

[||] School of Chemistry, The University of Melbourne.

[⊥] Commonwealth Scientific and Industrial Research Organization.

[1] Abbreviations: Aβ, β-amyloid; AAPH, 2,2-azobis(2-amidinopropane) dihydrochloride; apo, apolipoprotein; BSA, bovine serum albumin; LDL, low-density lipoprotein; oxLDL, oxidized low-density lipoprotein; SAP, serum amyloid P component; ThT, thioflavin T.

10.1021/bi050497v CCC: $30.25
Published on Web 06/04/2005

Proteins that form amyloid fibrils are diverse, typically sharing no significant sequence homology or native structure. Despite such diversity, amyloid precursor proteins self-associate and aggregate to form remarkably ordered structures with universal properties. Amyloid fibrils are structurally characterized by X-ray diffraction patterns, indicating β-sheets extending along the long axis of the fibril and a core structure composed of at least two β-sheets (*13*). This cross-β-structure provides amyloid fibrils with key diagnostic properties: the binding and alteration of the spectral properties of the dyes thioflavin T (ThT) and Congo Red. Another characteristic of amyloid is the recognition of fibrils by the plasma protein serum amyloid P component (SAP). SAP universally colocalizes with physiological amyloid deposits (*14*), including the cerebral amyloid of Alzheimer's disease (*15*). This association is attributed to the calcium-dependent binding of SAP to all amyloid fibrils tested thus far in vitro, regardless of the fibril precursor protein (*16*).

Many mechanisms have been proposed for the oxidative modification of LDL in vivo. Several act by the generation of free radicals, such as enzyme products of myeloperoxidase (*17*), 15-lipoxygenase (*18*), and nitric oxide synthase (*17*). In addition, cells of the immune system such as macrophages and polymorphonuclear leukocytes generate a variety of oxidants such as singlet oxygen ($^1O_2$*) and hydroxyl radicals ($^{\bullet}$OH) upon specific membrane perturbation (*19*). The Fenton reaction is commonly used to oxidize LDL in vitro using copper(II) ions as the oxidant (*19, 20*). Copper treatment of LDL generates particles with physical properties similar to LDL recovered from advanced atherosclerotic plaques, namely, increased electronegativity and protein fragmentation (*21, 22*). Organic compounds that generate free radicals [e.g., 2,2′-azobis(2-amidinopropane) hydrochloride (AAPH)] have also been used in vitro to oxidize lipoproteins (*23*).

The highly reactive oxidant ozone was recently identified in atherosclerotic plaque tissue (*24*). The proposed mechanism of ozone formation in atherosclerotic plaques is via the antibody-catalyzed water oxidation pathway (*25*). The mechanism of this reaction is proposed to proceed via a trioxygen intermediate such as dihydrogen trioxide (H_2O_3) or ozone (O_3). Double bonds of phospholipids and cholesterol in LDL are potential cleavage sites for ozone. Ozonolysis of phospholipids in aqueous solution produces hydrogen peroxide and an aldehyde (*26*), raising the possibility that radicals are generated indirectly. Ozone also reacts directly with proteins with a high affinity for sulfur-containing and aromatic side chains of amino acids (*27*). Incubation of macrophages with LDL modified by 5,6-*seco*sterol, a product of the reaction of ozone with cholesterol, induces lipid loading of macrophages to produce foam cells (*24*). These studies highlight the diverse mechanisms involved in LDL modification leading to accelerated lipid uptake by macrophages. Since the CD36 receptor binds amyloid fibrils, we considered whether the oxidation of LDL by copper ions, AAPH, or ozone generates amyloid-like structures and whether such structures might form a common basis for macrophage receptor recognition.

EXPERIMENTAL PROCEDURES

Materials. Human LDL was isolated from fresh plasma by preparative ultracentrifugation (*28*) or purchased from Biomedical Technologies Inc. (Stoughton, MA). Human SAP was purified from human serum (*29*) or purchased from Calbiochem. Human apoC-II amyloid fibrils were prepared as described previously (*29*). AAPH was purchased from Aldrich (Milwaukee, WI). ^{125}I-LDL was purchased from Biomedical Technologies Inc.

Oxidation of LDL. Three different methods were used to oxidize LDL. Copper- and AAPH-oxLDL were prepared by incubating LDL (20 μg/mL) in 20 mM Tris-HCl, 140 mM NaCl, and 0.1% (w/v) NaN_3, pH 7.4, with 10 μM $CuSO_4$ or 2 mM AAPH for 15 h at room temperature or 37 °C, respectively. LDL in 20 mM Tris-HCl, 140 mM NaCl, and 0.1% (w/v) NaN_3, pH 7.4, was treated at room temperature with ozone supplied by an ozone generator (Yanco Industries, Burton, Canada) at a flow rate of 125 mL/min with a discharge generating the equivalent of 5.8 mg of ozone/min. LDL samples (100 μL at 0.2 mg/mL) were treated with ozone for various periods as indicated for ThT studies. Gel filtration (1 mL at 0.2 mg/mL) and sedimentation velocity (380 μL at 0.2 mg/mL) samples were exposed to ozone for 4.5 and 1.7 min, respectively. Samples for X-ray diffraction (2.5 mL at 0.4 mg/mL) were treated for 22 min. OxLDL were analyzed by SDS gel electrophoresis using 15% Tris−glycine gels and Coomassie Blue R-250 staining.

Thioflavin T Reactivity. Samples of LDL (20 μg/mL) in 20 mM Tris-HCl, 140 mM NaCl, 0.1% (w/v) NaN_3, pH 7.4, and 8 μM ThT (final volume 250 μL) were added to microtiter wells. ThT fluorescence was monitored in 30 min intervals using a f_{max} platereader (Molecular Devices, Sunnyvale, CA) equipped with 444/485 nm excitation/emission filters. Fluorescence emission spectra were obtained for samples containing 8 μM ThT using a SPEX Fluorolog/Tau-2 spectrofluorometer and 5 mm path length cuvette. Excitation and emission slit widths were 2 nm.

Congo Red Reactivity. ApoC-II amyloid fibrils, LDL, and copper-oxLDL samples (0.2 mg/mL) were centrifuged at 435000*g* for 1 h in a Beckman TLA-100 ultracentrifuge (Beckman/Coulter, Fullerton, CA) at 20 °C. Aggregates were stained with 1 mM Congo Red for 1 h and collected by brief centrifugation at 300000*g*. Samples were resuspended in 80 μL of water and viewed under bright-field and cross-polarized light in a Olympus SZX12 microscope. Images were recorded with an Olympus DP10 camera.

Sedimentation Analysis. Sedimentation velocity analysis was performed using a Beckman model XL-A analytical ultracentrifuge at 20 °C as described previously (*29*). Native LDL and oxLDL samples were centrifuged at 40000 rpm with radial absorbance data acquired at 280 nm and radial increments of 0.002 cm in the continuous scanning mode. Where indicated, the concentrations of SAP, EDTA, and calcium were 60 μg/mL, 2 mM, and 2 mM, respectively. Radial scans were taken at 10 min intervals. Data were fitted to a continuous size distribution model using the program SEDFIT (*30*).

Size Exclusion Chromatography. Samples (1 mL) of native and oxLDL (20 μg/mL) were applied to a HR10-30 column packed with Sephacryl S-1000 gel filtration resin (Pharmacia Biotech, Uppsala, Sweden) equilibrated in 20 mM Tris-HCl, 140 mM NaCl, 2 mM $CaCl_2$, and 0.1% (w/v) NaN_3, pH 7.4. Samples were eluted at 2 mL/min. The eluate was mixed with 8 μM ThT and the fluorescence monitored using a SPEX Fluorolog/Tau-2 spectrofluorometer.

Electron Microscopy. Samples eluting from size exclusion chromatography were applied to freshly glow-discharged carbon-coated copper grids and negatively stained with 2% (w/v) potassium phosphotungstate, pH 6.8. Samples were examined using a FEI Tecnai 12 transmission electron microscope equipped with a Soft Imaging System MegaView III CCD camera. Micrographs were recorded at nominal magnifications of 150000×.

X-ray Diffraction Studies. OxLDL was concentrated to approximately 20 mg/mL (50 μL) in an Amicon Centricon (molecular mass cutoff 100000 kDa) by centrifugation at 1000 rpm at 15 °C in a Beckman GS6R benchtop centrifuge. The sample was diluted with water and centrifuged again under the same conditions to remove excess salt. Samples were drawn by capillary action into acid-washed quartz capillaries, placed onto the side of a 600 MHz NMR instrument, and allowed to dry for 1 week in an attempt to align the samples. X-rays were generated by a MAC Science SRA M18Xh1 rotating anode X-ray generator, operating at 40 kV and 22 mA with an AXCO CS-SRA-PX150 glass monocapillary focusing optic delivering a 120 μm spot on the sample. The images were collected on an R-axis II Image Plate X-ray detector.

Cellular Degradation, Binding, and Uptake Assays of Oxidized LDL. Elicited peritoneal macrophages were collected by peritoneal lavage 4 days after intraperitoneal injection of 6−8-week-old mice with 3% thioglycolate as we previously described (*12*, *31*). Cells were washed in phosphate-buffered saline, cultured for 2 h in DMEM with 5% FCS, and washed again to remove nonadherent cells. Adherent cells were incubated in DMEM with 5% FCS overnight prior to use and were routinely >95% $CD11b^+$ and $F4/80^+$ as determined by flow cytometric analysis. Measurements of ^{125}I-copper-oxLDL degradation and cell association (uptake and binding) were performed using confluent monolayers of peritoneal macrophages (7×10^5) in 24-well plates as previously described (*3*). Briefly, ^{125}I-copper-oxLDL was incubated alone or in the presence of a 30-fold excess of unlabeled copper-oxLDL competitor or 60 μg/mL SAP and 2 mM $CaCl_2$ or bovine serum albumin (BSA) for 10 min at room temperature. Cells were incubated with ligands for 5 h at 37 °C, and media were removed and assayed for TCA-soluble non-iodide degradation products (^{125}I-oxLDL degradation). Cells were washed three times with 50 mM Tris-HCl, pH 7.4, 0.15 M NaCl, and 2 mg/mL BSA, lysed in 0.1 M NaOH, and assayed for ^{125}I (^{125}I-oxLDL cell association) and cellular protein content. Cellular protein content was measured by BCA assay (Pierce, Rockford, IL), and data were expressed as nanograms of ^{125}I-oxLDL degraded or associated per milligram of protein. All measurements were performed in triplicate.

RESULTS

Thioflavin T Fluorescence of Oxidized LDL. We investigated the effect of copper and AAPH oxidation of LDL on its ability to alter the fluorescence of ThT. Incubation of LDL with copper or AAPH generated large, time-dependent increases in ThT reactivity (Figure 1A), indicative of the presence of amyloid-like structures. In contrast, native, nonoxidized LDL failed to generate significant ThT fluorescence when incubated over the same time course. Maximum ThT fluorescence for copper-treated LDL coincided with changes in absorbance at 234 nm, indicating the formation of conjugated dienes (*32*). SDS gel electrophoresis of copper-oxLDL indicated fragmentation of the protein component of LDL, apoB, as reported previously (*33*).

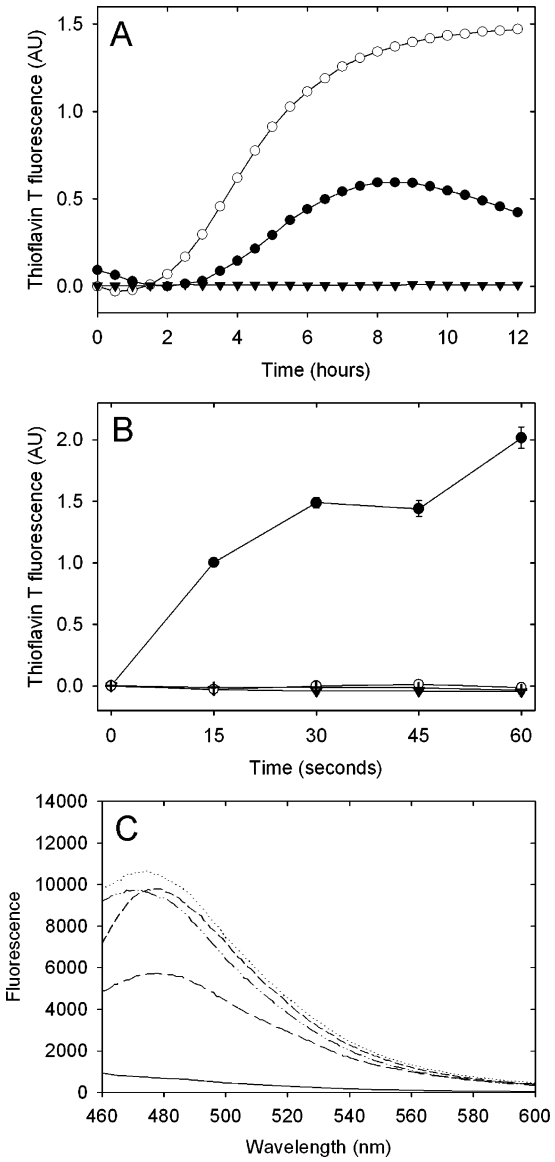

FIGURE 1: (A) ThT fluorescence for LDL incubated alone (closed triangles) or in the presence of 10 μM $CuSO_4$ (open circles) or 2 mM AAPH (closed circles). (B) ThT fluorescence of LDL oxidized by ozone. LDL and buffer alone were treated with ozone at a flow rate of 125 mL/min with an ozone discharge equivalent to 120 μmol/min (closed circles and closed triangles, respectively). Identical samples of LDL were treated with oxygen (open circles) or nitrogen (cross hair) at equivalent flow rates. (C) Fluorescence emission spectra (excitation 450 nm) for ThT in the presence of native LDL (solid line), copper-oxLDL (dotted line), AAPH-oxLDL (long dashed line), ozone-oxLDL (dash-dot-dotted line), or apolipoprotein C-II amyloid fibrils (short dashed line).

Large increases in ThT reactivity were also observed for LDL exposed to ozone for discrete periods of time over a 0−60 s range (Figure 1B). Unlike LDL oxidized by free radicals produced by copper and AAPH (Figure 1A), the increase in ThT fluorescence induced by a specific amount of ozone occurred almost instantaneously, consistent with the high reactivity of ozone. The increase was, however, dependent on the time of ozone exposure, increasing to a

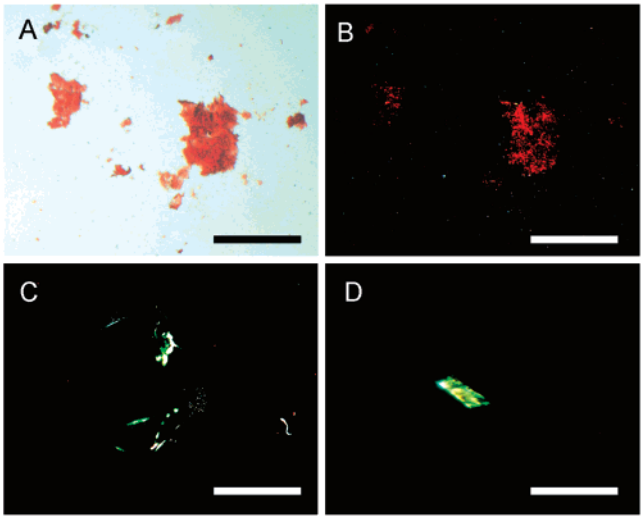

FIGURE 2: Effect of oxidation on the Congo Red optical birefringence of LDL. (A) Light microscopy of the native LDL pellet after Congo Red staining. Cross-polarized light microscopy of (B) native LDL, (C) apoC-II amyloid fibrils, and (D) copper-oxLDL. Scale bar = 6 μM.

point of apparent saturation. No significant ThT reactivity was observed for LDL treated with equivalent flow rates of oxygen or nitrogen gases or for buffer alone treated with ozone. SDS gel electrophoresis of ozone-treated LDL indicated extensive cleavage of apoB. The fluorescence emission spectra of ThT co-incubated with LDL oxidized by copper, AAPH, or ozone were similar and comparable to that of ThT co-incubated with apoC-II amyloid fibrils with the emission maximum in the range 479−482 nm (excitation 450 nm) (Figure 1C).

Congo Red Birefringence. Optical birefringence studies demonstrated that oxLDL also interacts with the diagnostic amyloid dye, Congo Red (Figure 2). Both oxLDL aggregates (Figure 2D) and apoC-II amyloid fibrils (Figure 2C) displayed strong apple green birefringence when viewed under cross-polarized light in the presence of Congo Red. Native LDL particles (Figure 2A,B) did not exhibit Congo Red birefringence under the same conditions.

Sedimentation Velocity Analysis of Oxidized LDL. The ability of oxLDL to alter the spectral properties of ThT and Congo Red indicated the presence of amyloid-like structures and prompted an investigation of the SAP binding properties of oxLDL. Sedimentation velocity profiles were obtained for native LDL in the presence and absence of SAP and calcium (Figure 3A,B). Under the conditions used, SAP alone sedimented with a sedimentation coefficient of approximately 7.0 S and contributed 20% to the total optical density. Comparison of the calculated sedimentation coefficient distributions for native LDL in the presence and absence of SAP (Figure 3B) demonstrated that SAP does not signifi-

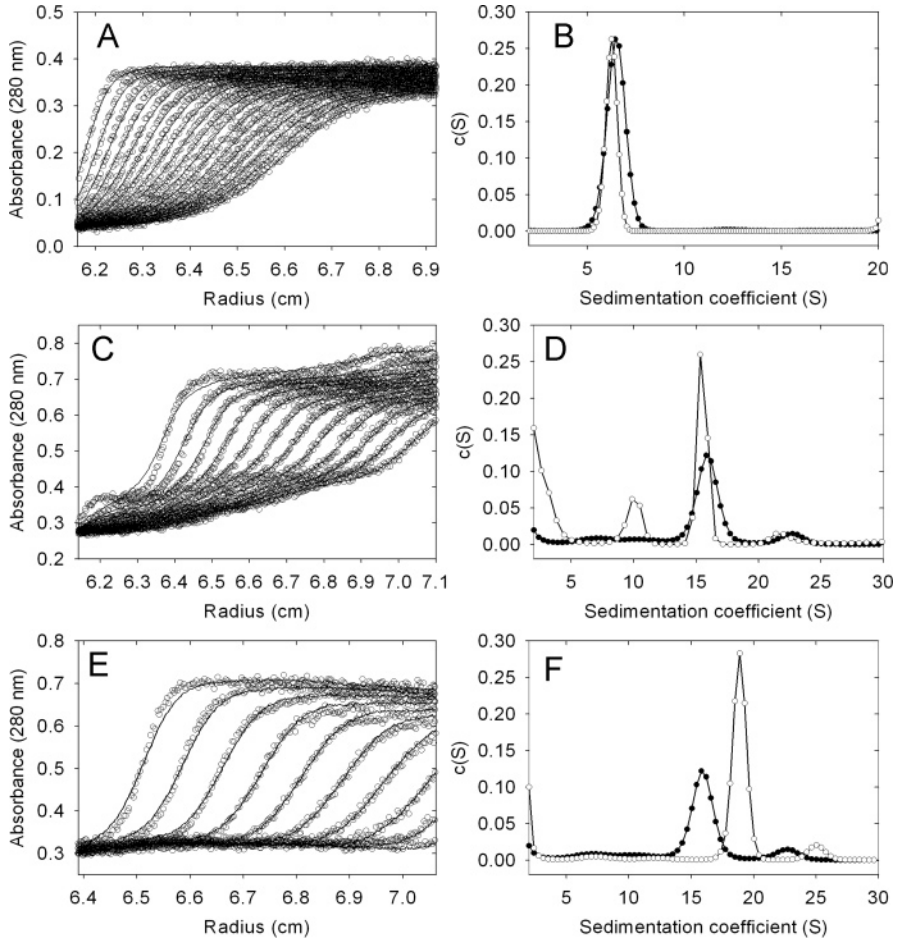

FIGURE 3: Sedimentation velocity analysis of (A) native LDL, (C) copper-oxLDL with SAP and EDTA, and (E) copper-oxLDL with SAP and calcium. Best fits from continuous sedimentation coefficient distribution analysis are represented as solid lines. Continuous sedimentation coefficient distributions for (B) native LDL alone (open circles) and with SAP and calcium (closed circles), (D) copper-oxLDL alone (closed circles) and with SAP and EDTA (open circles), and (F) copper-oxLDL alone (closed circles) and with SAP and calcium (open circles).

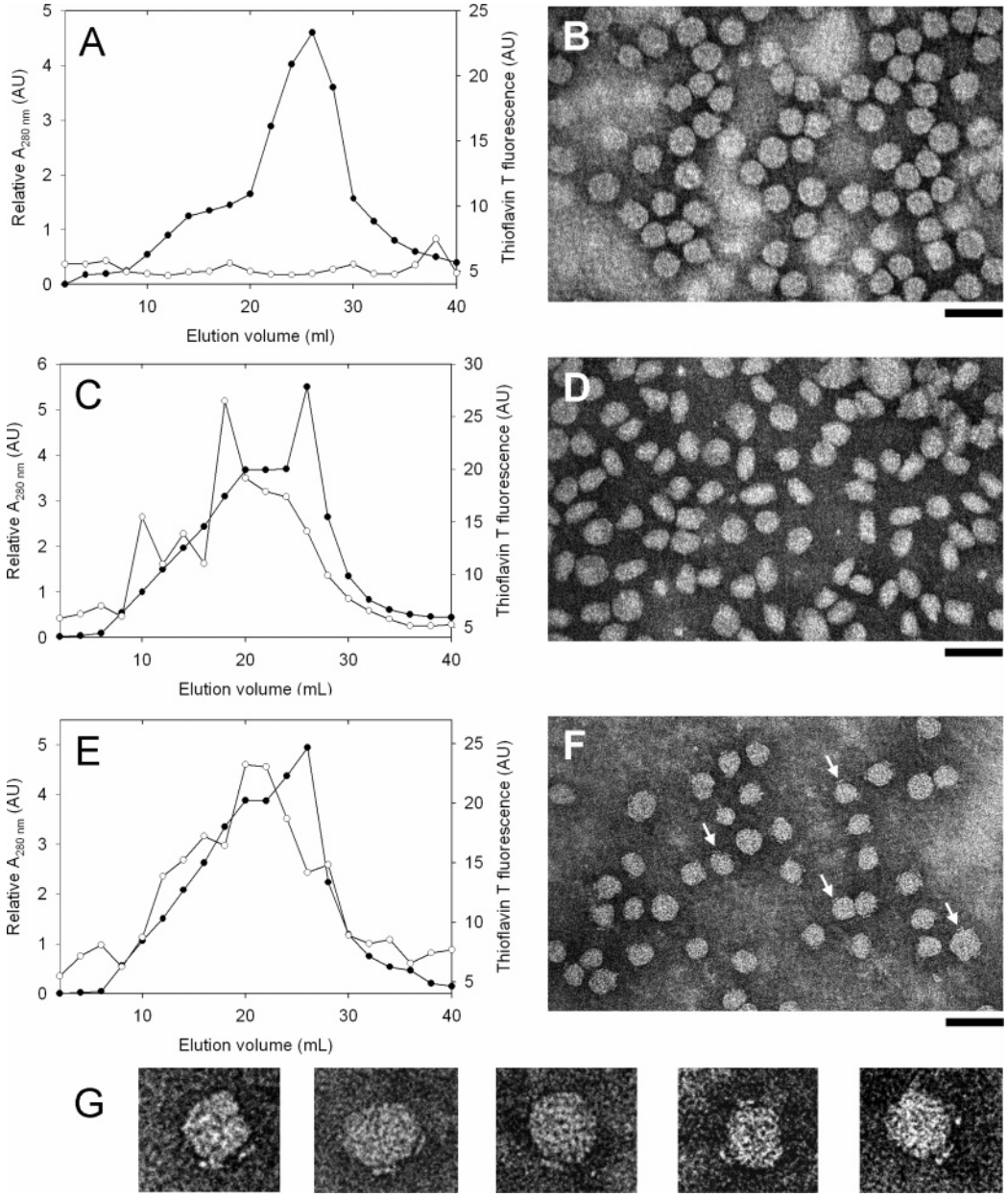

FIGURE 4: Size exclusion chromatography for (A) native LDL, (C) copper-oxLDL, and (E) copper-oxLDL and SAP (60 μg/mL). Eluates were monitored by absorbance at 280 nm (closed circles) and ThT reactivity (open circles). Samples eluting at the maximum of the absorbance peaks in (A, C, and E) were analyzed by transmission electron microscopy (B, D, and F, respectively). Arrows in (F) indicate SAP binding to copper-oxLDL. A collage of images from the sample in (F) is shown at higher magnification in (G). Scale bar = 50 nm.

cantly alter the rate of LDL sedimentation in the presence of calcium and, therefore, does not bind appreciably to native LDL. The sedimentation profile of copper-oxLDL particles incubated with SAP and EDTA (Figure 3C) showed three discrete sedimenting species. Continuous size distribution analysis identified major sedimenting species at 16 and 23 S, with an additional small population of sedimenting material at 10 S, attributed to SAP in the absence of calcium (Figure 3D). The presence of the 23S species is consistent with the formation of a dimeric species in oxLDL which is not evident in the native LDL sample (Figure 3B). The unchanged sedimentation rate of copper-oxLDL in the presence of SAP and EDTA when compared to copper-oxLDL alone, coupled with the discrete sedimentation profile of SAP, suggested that SAP does not bind oxLDL in the absence of calcium. The sedimentation profile of copper-oxLDL incubated with SAP and calcium displayed noticeable increases in the rate of boundary movement of the sedimenting species (Figure 3E). Continuous size distribution analysis (Figure 3F) showed that incubation with SAP and calcium increased the modal *S* values of both 16S and 23S oxLDL populations. No significant peak corresponding to SAP alone in this sample was observed, suggesting that little free SAP remained in solution under these conditions. Together, these results suggest that SAP binds to the sedimenting component of copper-oxLDL in a calcium-dependent manner. The rate of sedimentation of ozone-oxLDL was also increased significantly by the addition of SAP in the presence of calcium (data not shown), indicating that both copper and ozone-induced oxidation of LDL promotes SAP binding.

Sedimentation velocity analysis was used to examine the extent of lipid loss incurred by LDL as a result of copper-mediated oxidation. Sedimentation coefficients for the main

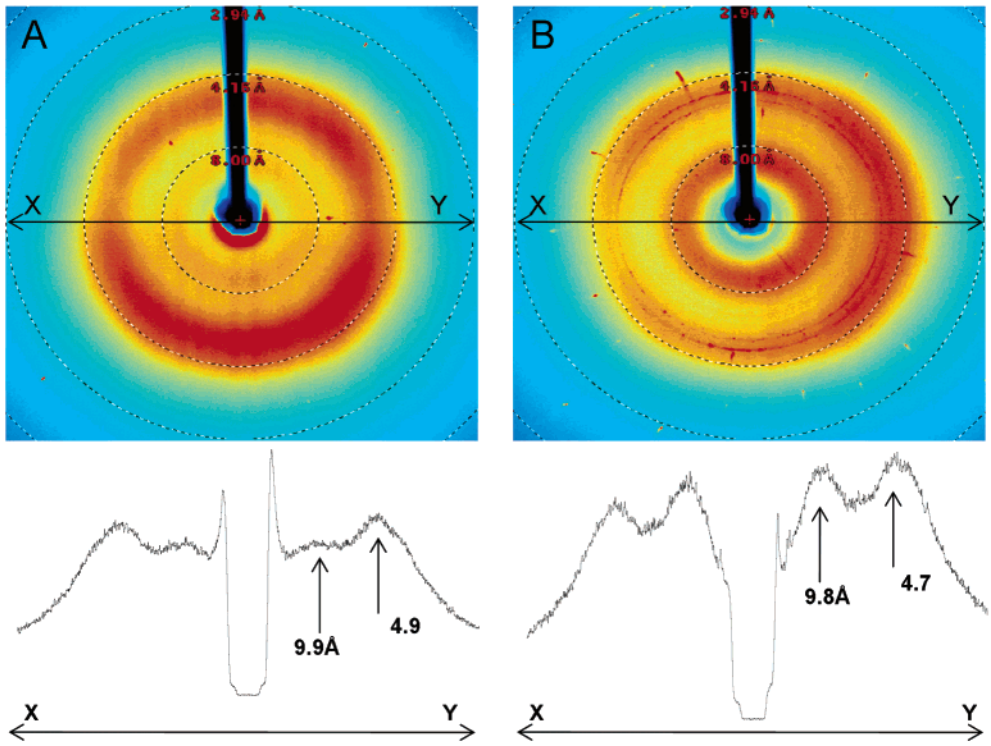

FIGURE 5: X-ray diffraction patterns from (A) native and (B) ozone-oxLDL. The upper panels are false color diffraction images obtained from a 12 h exposure of the material in a 1 mm glass capillary, at 100 mm from the sample, and the lower panels are intensity profiles cut horizontally across the images along the $X-Y$ line between the 2.94 Å resolution limits.

population of sedimenting species in native LDL and copper-oxLDL were determined in solutions containing different concentrations of H_2O and D_2O. Interpolation of the data to determine the solution density required for zero sedimentation yielded average densities of 1.04 g/mL for native LDL and 1.10 g/mL for copper-oxLDL. The increased particle density of copper-oxLDL indicates a significant loss of lipid from LDL during copper-mediated oxidation. Sedimentation velocity analysis of AAPH- and ozone-treated LDL also indicated increased rates of sedimentation compared to native LDL, consistent with a loss of lipid from the particle as a consequence of oxidation.

Gel Filtration and Electron Microscopy of SAP and Oxidized LDL Complexes. Sedimentation velocity analysis of copper-oxLDL indicated a population of dense, faster sedimenting species together with a significant amount of nonsedimenting material (Figure 3). To identify the ThT-reactive species within copper-oxLDL, samples were subjected to size exclusion chromatography, and the eluate was assayed for absorbance at 280 nm and ThT reactivity (Figure 4). Native LDL eluted with negligible ThT fluorescence (Figure 4A) and displayed spherical morphologies by negative staining electron microscopy (Figure 4B). Copper-oxLDL, both in the presence and in the absence of SAP and calcium, eluted with major peaks at approximately 26 mL. Comparison of the absorbance and ThT reactivity elution profiles (Figure 4C,E) shows that copper-induced ThT reactivity is associated with material eluting within the LDL size range. Gel filtration profiles for ozone-oxLDL yielded similar results, indicating that the ThT reactivity of ozone-oxLDL is also associated with large molecular species. Copper-oxLDL obtained from the peak in the absorbance profile in Figure 4C had a less spherical appearance and were generally smaller and more heterogeneous than native LDL (compare Figure 4B with Figure 4D,F). Copper-oxLDL co-incubated with SAP and calcium (Figure 4F) showed consistent binding of SAP to the LDL surface, as indicated more clearly at higher magnification (Figure 4G). The length of the negatively stained material associated with oxLDL particles was consistent with the diameter of SAP pentamers measured in samples of SAP alone. To further determine the nature of the ThT-reactive component in oxLDL, we extracted the lipid from copper-oxLDL and tested the sonicated lipid extract for ThT fluorescence. Negligible fluorescence was detected, suggesting that the ThT reactivity of copper-oxLDL arises primarily from the protein component.

X-ray Diffraction. We sought to confirm the presence of amyloid-like structures on oxLDL using X-ray diffraction. Figure 5 shows powder diffraction patterns for native (Figure 5A) and ozone-oxLDL (Figure 5B). The anisotropy of the broad diffraction rings is attributable to nonuniformity of the sample in the capillary. The results for native LDL show a diffuse powder diffraction ring with maximum intensity corresponding to an atomic spacing of ~4.7 Å, consistent with the spacing between β-strands in a β-sheet. Ozone treatment of LDL generates an additional diffuse powder diffraction ring with maximum intensity indicating a spacing of ~9.8 Å. This distance is characteristic of cross-β-structure (*13*), a defining characteristic of amyloid. Aligned amyloid fibrils show a clear distinction in the intensity of the equatorial and meridonal intensities (*13*). While the data in Figure 5B do not meet this strict definition for a cross-β-structure, this may be attributable to the difficulty in aligning a sample composed largely of spherical particles (Figure 4).

Effect of SAP on the Uptake of Copper-Oxidized LDL by Macrophages. To probe the physiological implications of the extensive binding of SAP to copper-oxLDL, we assayed

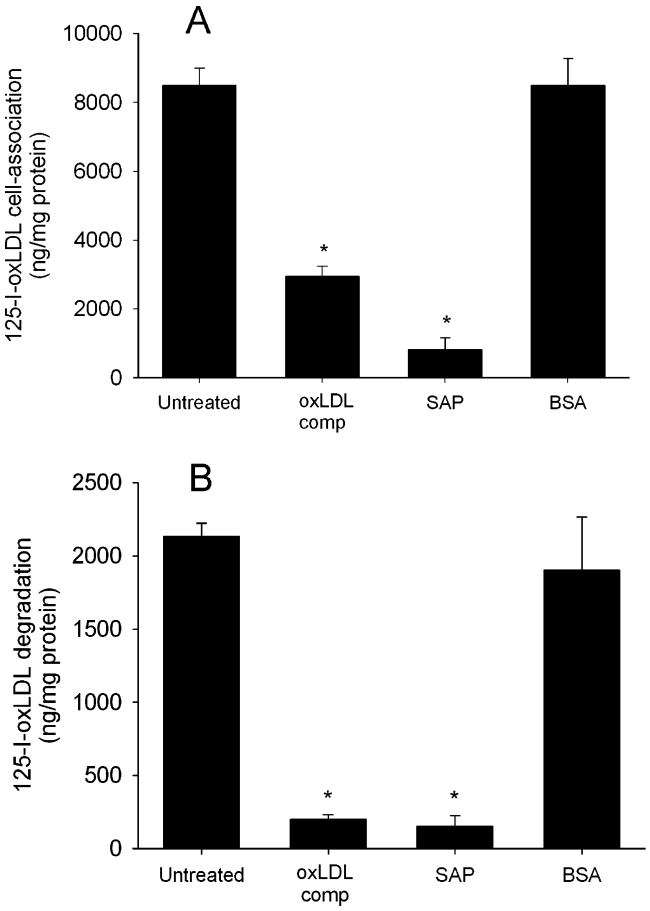

FIGURE 6: SAP inhibits cellular metabolism of copper-oxLDL. (A) ^{125}I-copper-oxLDL bound and internalized by peritoneal macrophages was measured after 5 h incubation alone (untreated) or in the presence of a 30-fold excess of unlabeled copper-oxLDL competitor or 60 μg/mL SAP or BSA. (B) Lysosomal degradation of ^{125}I-copper-oxLDL was measured in peritoneal macrophages incubated with ^{125}I-copper-oxLDL alone (untreated) or in the presence of a 30-fold excess of unlabeled copper-oxLDL competitor or 60 g/mL SAP or 60 g/mL BSA. Data are presented as the mean of triplicate samples (standard deviation, * = $p \leq 0.005$).

the receptor-mediated uptake of copper-oxLDL by peritoneal macrophages, both in the absence and in the presence of SAP (Figure 6). ^{125}I-Labeled copper-oxLDL was employed to monitor the effect of SAP binding on the cellular association, in addition to the degradation of copper-oxLDL by peritoneal macrophages. The association and internalization of copper-oxLDL are dramatically diminished in samples co-incubated with either SAP or a 30-fold excess of unlabeled oxLDL (Figure 6A). Following 5 h of incubation, receptor-mediated uptake is reduced by more than 90% for copper-oxLDL samples bound to SAP. BSA at comparable concentrations had no effect on the association of copper-oxLDL with macrophages. Lysosomal degradation of ^{125}I-copper-oxLDL by peritoneal macrophages was inhibited by SAP in a similar fashion (Figure 6B).

DISCUSSION

Our results show that the oxidation of LDL by copper ions, AAPH, or ozone is accompanied by the formation of amyloid-like structures in oxLDL as monitored by thioflavin T fluorescence, Congo Red birefringence, SAP binding, and a characteristic X-ray diffraction pattern. These results are supported by previous studies using IR spectroscopy (*34*), circular dichroism (*35*), and synchrotron X-ray scattering (*36*) that demonstrate significant protein conformational changes associated with LDL oxidation. It is therefore of interest to speculate on the basis for the observed changes. While the huge size and nature of apoB-100 have precluded detailed structural studies, computational analyses of the secondary structure of apoB suggest a pentapartite structure composed of both amphipathic α-helical domains and amphipathic β-stranded domains (*37*). One explanation for the generation of cross-β-structure is that oxidation leads to lipid modification and loss of lipid from the LDL particle as deduced from the increased particle density of oxLDL determined from sedimentation velocity measurements. Shrinkage of the core lipid component might impose conformation constraint on the β-stranded domain leading to the formation of amyloid-like cross-β-structure. Such a mechanism has recently been proposed to explain the activating effect of lipid on the formation of amyloid fibrils composed of islet amyloid polypeptide (*38*). Support for this explanation also comes from studies on the effect of phospholipase A2 on LDL. Phospholipase A2 treatment of LDL generates electronegative particles with increased immunoreactivity to an amyloid oligomer-specific antibody and increased β-strand content (*39*). These electronegative particles resemble a subpopulation of plasma small dense LDL enriched in lipid peroxides. Lipid loss associated with the induction of cross-β-structure and recognition by macrophages would also account for the increased atherogenicity of LDL treated with sphingomyelinase (*7*) or lipoprotein lipase (*8*).

In the case of LDL oxidation, other explanations for the presence of amyloid structures may be considered. Oxidation of LDL is accompanied by significant covalent modification of both the lipid and protein components. Synchrotron X-ray scattering studies of LDL during copper oxidation indicate that oxidation first affects the outer shell of the surface phospholipids and then it spreads to damage of apoB and the internal lipid core of LDL (*36*, *40*, *41*). During LDL oxidation there is a progressive decrease in the number of reactive lysine ϵ groups, attributed to blocking of amino groups by reaction with short-chain aldehydes derived from peroxidation of polyunsaturated fatty acids such as malondialdehyde or 4-hydroxynonenal (*40*). These oxidative processes, leading to covalent modification and cleavage of both the lipid and protein components of LDL, could lead directly to the formation of amyloid-like structures. Several studies provide support for this mechanism. Phospholipid adducts of apoB have been identified in oxLDL and are recognized by specific monoclonal antibodies that block the uptake of oxLDL by CD36 transfected COS-7 cells (*4*). Oxidized lipid products derived from cholesterol and fatty acids covalently modify Aβ and dramatically accelerate amyloid fibril formation (*42*). Solid-state NMR demonstrates that acylation of Aβ peptides by fatty acids affects the amyloid folding pathway and resulting fibril morphology (*43*). These potential effects of oxidized lipids on the induction of cross-β-structure in LDL are not necessarily mutually exclusive to separate effects attributable to changes in the size of the LDL lipid core.

The results in Figure 6 showing that SAP inhibits the uptake of oxLDL by macrophages may be considered in relation to recent studies on C-reactive protein (CRP). CRP is an acute-phase reactant that resembles SAP in that both

proteins belong to the highly conserved pentraxin family of plasma proteins and serve as a pattern recognition molecule in the innate immune system. Plasma levels of CRP are an independent and powerful risk factor for atherosclerosis. CRP binds to oxLDL but not to native LDL (*44*) and interacts with enzymically degraded LDL to enhance complement activation in human serum (*45*). Thus, during inflammation, the clearance of CRP-opsonized particles would be predicted to enhance the clearance of modified LDL via phagocytic complement receptors (*46*). In this regard, SAP and CRP may have opposing effects on the uptake of oxLDL by macrophages.

The macrophage CD36 receptor binds fibrillar β-amyloid and apoC-II fibrils, initiating a proinflammatory signaling cascade. The discovery of amyloid-like structures in oxLDL identifies a common mechanism by which CD36 may recognize these diverse ligands. The binding of these structures by SAP may sequester these proinflammatory structures and prevent the induction of signal transduction pathways that lead to tissue damage, inflammation, and the progression of atherosclerosis.

ACKNOWLEDGMENT

We are grateful to Leanne Wilson for valuable suggestions during the preparation of the manuscript.

REFERENCES

1. Goldstein, J. L., Ho, Y. K., Basu, S. K., and Brown, M. S. (1979) Binding site on macrophages that mediates uptake and degradation of acetylated low density lipoprotein, producing massive cholesterol deposition, *Proc. Natl. Acad. Sci. U.S.A. 76*, 333−337.
2. Suzuki, H., Kurihara, Y., Takeya, M., Kamada, N., Kataoka, M., Jishage, K., Ueda, O., Sakaguchi, H., Higashi, T., Suzuki, T., Takashima, Y., Kawabe, Y., Cynshi, O., Wada, Y., Honda, M., Kurihara, H., Aburatani, H., Doi, T., Matsumoto, A., Azuma, S., Noda, T., Toyoda, Y., Itakura, H., Yazaki, Y., Kodama, T., et al. (1997) A role for macrophage scavenger receptors in atherosclerosis and susceptibility to infection, *Nature 386*, 292−296.
3. Kunjathoor, V. V., Febbraio, M., Podrez, E. A., Moore, K. J., Andersson, L., Koehn, S., Rhee, J. S., Silverstein, R., Hoff, H. F., and Freeman, M. W. (2002) Scavenger receptors class A-I/II and CD36 are the principal receptors responsible for the uptake of modified low density lipoprotein leading to lipid loading in macrophages, *J. Biol. Chem. 277*, 49982−49988.
4. Boullier, A., Gillotte, K. L., Horkko, S., Green, S. R., Friedman, P., Dennis, E. A., Witztum, J. L., Steinberg, D., and Quehenberger, O. (2000) The binding of oxidized low density lipoprotein to mouse CD36 is mediated in part by oxidized phospholipids that are associated with both the lipid and protein moieties of the lipoprotein, *J. Biol. Chem. 275*, 9163−9169.
5. Clarke, R., and Armitage, J. (2002) Antioxidant vitamins and risk of cardiovascular disease. Review of large-scale randomised trials, *Cardiovasc. Drugs Ther. 16*, 411−415.
6. Khoo, J. C., Miller, E., McLoughlin, P., and Steinberg, D. (1988) Enhanced macrophage uptake of low density lipoprotein after self-aggregation, *Arteriosclerosis 8*, 348−358.
7. Marathe, S., Choi, Y., Leventhal, A. R., and Tabas, I. (2000) Sphingomyelinase converts lipoproteins from apolipoprotein E knockout mice into potent inducers of macrophage foam cell formation, *Arterioscler. Thromb. Vasc. Biol. 20*, 2607−2613.
8. Babaev, V. R., Fazio, S., Gleaves, L. A., Carter, K. J., Semenkovich, C. F., and Linton, M. F. (1999) Macrophage lipoprotein lipase promotes foam cell formation and atherosclerosis in vivo, *J. Clin. Invest. 103*, 1697−1705.
9. Moore, K. J., El Khoury, J., Medeiros, L. A., Terada, K., Geula, C., Luster, A. D., and Freeman, M. W. (2002) A CD36-initiated signaling cascade mediates inflammatory effects of beta-amyloid, *J. Biol. Chem. 277*, 47373−47379.
10. Febbraio, M., Hajjar, D. P., and Silverstein, R. L. (2001) CD36: a class B scavenger receptor involved in angiogenesis, atherosclerosis, inflammation, and lipid metabolism, *J. Clin. Invest. 108*, 785−791.
11. Kunjathoor, V. V., Tseng, A. A., Medeiros, L. A., Khan, T., and Moore, K. J. (2004) beta-Amyloid promotes accumulation of lipid peroxides by inhibiting CD36-mediated clearance of oxidized lipoproteins, *J. Neuroinflammation 1*, 23.
12. Medeiros, L. A., Khan, T., El Khoury, J. B., Pham, C. L., Hatters, D. M., Howlett, G. J., Lopez, R., O'Brien, K. D., and Moore, K. J. (2004) Fibrillar amyloid protein present in atheroma activates CD36 signal transduction, *J. Biol. Chem. 279*, 10643−10648.
13. Serpell, L. C., Fraser, P. E., and Sunde, M. (1999) X-ray fiber diffraction of amyloid fibrils, *Methods Enzymol. 309*, 526−536.
14. Pepys, M. B., Rademacher, T. W., Amatayakul-Chantler, S., Williams, P., Noble, G. E., Hutchinson, W. L., Hawkins, P. N., Nelson, S. R., Gallimore, J. R., Herbert, J., et al. (1994) Human serum amyloid P component is an invariant constituent of amyloid deposits and has a uniquely homogeneous glycostructure, *Proc. Natl. Acad. Sci. U.S.A. 91*, 5602−5606.
15. Coria, F., Castano, E., Prelli, F., Larrondo-Lillo, M., van Duinen, S., Shelanski, M. L., and Frangione, B. (1988) Isolation and characterization of amyloid P component from Alzheimer's disease and other types of cerebral amyloidosis, *Lab. Invest. 58*, 454−458.
16. Danielsen, B., Sorensen, I. J., Nybo, M., Nielsen, E. H., Kaplan, B., and Svehag, S. E. (1997) Calcium-dependent and -independent binding of the pentraxin serum amyloid P component to glycosaminoglycans and amyloid proteins: enhanced binding at slightly acid pH, *Biochim. Biophys. Acta 1339*, 73−78.
17. Carr, A. C., McCall, M. R., and Frei, B. (2000) Oxidation of LDL by myeloperoxidase and reactive nitrogen species: reaction pathways and antioxidant protection, *Arterioscler. Thromb. Vasc. Biol. 20*, 1716−1723.
18. Cathcart, M. K., and Folcik, V. A. (2000) Lipoxygenases and atherosclerosis: protection versus pathogenesis, *Free Radical Biol. Med. 28*, 1726−1734.
19. Frei, B., Stocker, R., and Ames, B. N. (1988) Antioxidant defenses and lipid peroxidation in human blood plasma, *Proc. Natl. Acad. Sci. U.S.A. 85*, 9748−52.
20. Fu, S., Davies, M. J., Stocker, R., and Dean, R. T. (1998) Evidence for roles of radicals in protein oxidation in advanced human atherosclerotic plaque, *Biochem. J. 333* (Part 3), 519−525.
21. Suarna, C., Dean, R. T., May, J., and Stocker, R. (1995) Human atherosclerotic plaque contains both oxidized lipids and relatively large amounts of alpha-tocopherol and ascorbate, *Arterioscler. Thromb. Vasc. Biol. 15*, 1616−1624.
22. Steinbrecher, U. P., Parthasarathy, S., Leake, D. S., Witztum, J. L., and Steinberg, D. (1984) Modification of low density lipoprotein by endothelial cells involves lipid peroxidation and degradation of low density lipoprotein phospholipids, *Proc. Natl. Acad. Sci. U.S.A. 81*, 3883−3887.
23. Thomas, M. J., Chen, Q., Zabalawi, M., Anderson, R., Wilson, M., Weinberg, R., Sorci-Thomas, M. G., and Rudel, L. L. (2001) Is the oxidation of high-density lipoprotein lipids different than the oxidation of low-density lipoprotein lipids?, *Biochemistry 40*, 1719−1724.
24. Wentworth, P., Jr., Nieva, J., Takeuchi, C., Galve, R., Wentworth, A. D., Dilley, R. B., DeLaria, G. A., Saven, A., Babior, B. M., Janda, K. D., Eschenmoser, A., and Lerner, R. A. (2003) Evidence for ozone formation in human atherosclerotic arteries, *Science 302*, 1053−1056.
25. Babior, B. M., Takeuchi, C., Ruedi, J., Gutierrez, A., and Wentworth, P., Jr. (2003) Investigating antibody-catalyzed ozone generation by human neutrophils, *Proc. Natl. Acad. Sci. U.S.A. 100*, 3031−3034.
26. Santrock, J., Gorski, R. A., and O'Gara, J. F. (1992) Products and mechanism of the reaction of ozone with phospholipids in unilamellar phospholipid vesicles, *Chem. Res. Toxicol. 5*, 134−141.
27. Mudd, J. B., Dawson, P. J., Tseng, S., and Liu, F. P. (1997) Reaction of ozone with protein tryptophans: band III, serum albumin, and cytochrome C, *Arch. Biochem. Biophys. 338*, 143−149.
28. Havel, R. J., Eder, H. A., and Bragdon, J. H. (1955) The distribution and chemical composition of ultracentrifugally separated lipoproteins in human serum, *J. Clin. Invest. 34*, 1345−1353.

29. MacRaild, C. A., Stewart, C. R., Mok, Y. F., Gunzburg, M. J., Perugini, M. A., Lawrence, L. J., Tirtaatmadja, V., Cooper-White, J. J., and Howlett, G. J. (2004) Non-fibrillar components of amyloid deposits mediate the self-association and tangling of amyloid fibrils, *J. Biol. Chem. 279*, 21038−21045.
30. Schuck, P. (2000) Size-distribution analysis of macromolecules by sedimentation velocity ultracentrifugation and lamm equation modeling, *Biophys. J. 78*, 1606−1619.
31. El Khoury, J. B., Moore, K. J., Means, T. K., Leung, J., Terada, K., Toft, M., Freeman, M. W., and Luster, A. D. (2003) CD36 mediates the innate host response to beta-amyloid, *J. Exp. Med. 197*, 1657−1666.
32. Esterbauer, H., Jurgens, G., Quehenberger, O., and Koller, E. (1987) Autoxidation of human low density lipoprotein: loss of polyunsaturated fatty acids and vitamin E and generation of aldehydes, *J. Lipid Res. 28*, 495−509.
33. Kawabe, Y., Cynshi, O., Takashima, Y., Suzuki, T., Ohba, Y., and Kodama, T. (1994) Oxidation-induced aggregation of rabbit low-density lipoprotein by azo initiator, *Arch. Biochem. Biophys. 310*, 489−496.
34. Gallego-Nicasio, J., Lopez-Rodriguez, G., Martinez, R., Tarancon, M. J., Fraile, M. V., and Carmona, P. (2003) Structural changes of low density lipoproteins with Cu^{2+} and glucose induced oxidation, *Biopolymers 72*, 514−520.
35. Brunelli, R., Mei, G., Krasnowska, E. K., Pierucci, F., Zichella, L., Ursini, F., and Parasassi, T. (2000) Estradiol enhances the resistance of LDL to oxidation by stabilizing apoB-100 conformation, *Biochemistry 39*, 13897−13903.
36. Meyer, D. F., Nealis, A. S., Macphee, C. H., Groot, P. H., Suckling, K. E., Bruckdorfer, K. R., and Perkins, S. J. (1996) Time-course studies by synchrotron X-ray solution scattering of the structure of human low-density lipoprotein during Cu(2+)-induced oxidation in relation to changes in lipid composition, *Biochem. J. 319* (Part 1), 217−227.
37. Hevonoja, T., Pentikainen, M. O., Hyvonen, M. T., Kovanen, P. T., and Ala-Korpela, M. (2000) Structure of low density lipoprotein (LDL) particles: basis for understanding molecular changes in modified LDL, *Biochim. Biophys. Acta 1488*, 189−210.
38. Knight, J. D., and Miranker, A. D. (2004) Phospholipid catalysis of diabetic amyloid assembly, *J. Mol. Biol. 341*, 1175−1187.
39. Asatryan, L., Hamilton, R. T., Isas, J. M., Hwang, J., Kayed, R., and Sevanian, A. (2005) LDL phospholipid hydrolysis produces modified electronegative particles with an unfolded apoB-100 protein, *J. Lipid Res. 46*, 115−122.
40. Gillotte, K. L., Horkko, S., Witztum, J. L., and Steinberg, D. (2000) Oxidized phospholipids, linked to apolipoprotein B of oxidized LDL, are ligands for macrophage scavenger receptors, *J. Lipid Res. 41*, 824−833.
41. Fruebis, J., Parthasarathy, S., and Steinberg, D. (1992) Evidence for a concerted reaction between lipid hydroperoxides and polypeptides, *Proc. Natl. Acad. Sci. U.S.A. 89*, 10588−10592.
42. Zhang, Q., Powers, E. T., Nieva, J., Huff, M. E., Dendle, M. A., Bieschke, J., Glabe, C. G., Eschenmoser, A., Wentworth, P., Jr., Lerner, R. A., and Kelly, J. W. (2004) Metabolite-initiated protein misfolding may trigger Alzheimer's disease, *Proc. Natl. Acad. Sci. U.S.A. 101*, 4752−4757.
43. Gordon, D. J., Balbach, J. J., Tycko, R., and Meredith, S. C. (2004) Increasing the amphiphilicity of an amyloidogenic peptide changes the beta-sheet structure in the fibrils from antiparallel to parallel, *Biophys. J. 86*, 428−434.
44. Chang, M. K., Binder, C. J., Torzewski, M., and Witztum, J. L. (2002) C-reactive protein binds to both oxidized LDL and apoptotic cells through recognition of a common ligand: Phosphorylcholine of oxidized phospholipids, *Proc. Natl. Acad. Sci. U.S.A. 99*, 13043−13048.
45. Bhakdi, S., Torzewski, M., Klouche, M., and Hemmes, M. (1999) Complement and atherogenesis: binding of CRP to degraded, nonoxidized LDL enhances complement activation, *Arterioscler. Thromb. Vasc. Biol. 19*, 2348−2354.
46. Mold, C. (1999) Role of complement in host defense against bacterial infection, *Microbes Infect. 1*, 633−638.

BI050497V